VI International Conference on Computational Methods for Coupled Problems in Science and Engineering
COUPLED PROBLEMS 2015
B. Schrefler, E. Oñate and M. Papadrakakis (Eds)

HYBRID SIMULATION OF HEAT TRANSFER PROBLEMS IN STRUCTURAL APPLICATIONS – COUPLED PROBLEMS 2015

GIUSEPPE ABBIATI*, ORESTE S. BURSI†, BOZIDAR STOJADINOVIC*, NICOLA TONDINI† AND CATHERINE WHYTE*

* Department of Civil, Environmental and Geomatic Engineering (D-BAUG), IBK, ETH Zurich
Stefano-Franscini-Platz 5, 8093 Zürich, Switzerland
e-mail: abbiati@ibk.baug.ethz.ch, whyte@ibk.baug.ethz.ch, stojadinovic@ibk.baug.ethz.ch

† Department of Civil, Environmental and Mechanical Engineering, University of Trento
Via Mesiano 77, 38123, Trento, Italy
email: oreste.bursi@unitn.it, nicola.tondini@unitn.it

Key words: Hybrid simulation, truss structures, thermal analysis, electric furnaces.

Abstract. The present paper presents all research activities focused on the development of a pure thermal hybrid simulator (THS). In detail, the need for a rigorous coupling is investigated, i.e. temperatures are sent from the numerical substructure (NS) to the physical substructure (PS) and interface heat fluxes are sent back from the PS to the NS. In this respect, a realistic benchmark case study is presented. It consists of a 2D truss bridge where a single truss element is "physically" substructured. In the current preliminary phase, an additional multiphysics FE code, COMSOL, is utilized to simulate the thermal response of this "experimental" substructure inside the electric furnace. In detail, two variants of the same case study are presented and characterized by two significantly different average thermal diffusivities. This approach provides a realistic insight into the capabilities of THS. Moreover, the present study paves the way for the implementation of a fully coupled thermomechanical hybrid simulation (TMHS), which account for indirect actions owing to restrained thermal deformations on the hot NS.

1 INTRODUCTION

Large-scale structural fire tests are rare because they are costly and require specialized facilities. As a result, most of the research regarding the behavior of structures in fire has been carried out on single structural components. These component tests do not provide insight into the thermomechanical interaction problem of the selected structural component with the remainder of the structure. In fact, statically indeterminate structural assemblies subjected to thermal loads experience indirect actions due to restrained thermal deformations. The hybrid simulation technique, extensively investigated in the mechanical domain, can be extended to the thermal field through temperature controlled furnaces and, thus, account for such a thermomechanical interaction. The first hybrid fire test (HFT) was performed by Mostafaei [1,2]. The PS was a first story column of a six-story reinforced concrete building, exposed to both axial and thermal loads in a vertical furnace. In order to simulate the fire development, a standard ASTM E119 fire curve was applied to both the column specimen and the numerical model of the remaining building, i.e. the NS implemented in the SAFIR FE Code [3]. However, the process was not

automated. A fully automated thermomechanical hybrid simulator (TMHS) developed by Whyte et al. [4] extended the scope of the well-known OpenFresco hybrid simulation framework [5] to include the temperature Degree-of-Freedom (DoF) and modeled the NS in the OpenSees FE code [6]. They validated their implementation on a Single-DoF two-element hybrid model. However, since OpenSees is a pure mechanical FE solver, the heat transfer dynamics was not accounted for on the numerical side. According to the state of the art, there remains a lack of a hybrid simulation (HS) environment where a substructure thermal coupling encompasses the whole domain, i.e. numerical and physical substructures. Along this line, the present paper describes research activities focused on the development of a pure thermal hybrid simulator (THS), which paves the way for simulating hot NSs for the purpose of TMHS.

2 GOVERNING EQUATIONS OF THERMOELASTICITY

First, the governing equations of thermoelasticity that define the coupled thermomechanical problem for a linear elastic isotropic continuum are briefly introduced [7]. The theory of thermoelasticity consists of i) the equilibrium equation;

$$\sigma_{ij,j} + X_i = \rho \ddot{u}_i \tag{1}$$

where σ_{ij} is the stress, X_i is the body force, ρ is the density and $\ddot{u}_i$ is the displacement.
ii) the heat transfer equation and iii) Fourier's heat conduction law:

$$\rho c_p \dot{\theta} - k\theta_{,ii} + \theta_0 \left(1 + \frac{\theta - \theta_0}{\theta_0}\right) \beta \dot{\varepsilon}_{ii} = Q \tag{2}$$

$$q_i = -k\theta_{,j} \tag{3}$$

where, k is the thermal conductivity, c_p is the specific heat at constant pressure, β represents the thermal expansion material constant, $\dot{\varepsilon}_{ij}$ the strain, Q is the heat source per unit volume, θ represents the temperature, θ_0 the reference temperature and q_i is the heat flux. Then, for a linear elastic behavior the constitutive equations read:

$$\varepsilon_{ij} = \frac{1}{2G}\left[\sigma_{ij} - \frac{\nu}{1+\nu}\sigma_{kk}\delta_{ij}\right] + \alpha \cdot (\theta - \theta_0)\,\delta_{ij} \tag{4}$$

where σ_{ij} and ε_{ij} are the generic stress and the strain tensor components, respectively; G is the tangent elastic modulus, whilst υ is the Poisson ratio and $\alpha = \beta/E$ is the thermal dilatation coefficient. The thermoelastic problem - Eqn. (1-4) - is solved by prescribing boundary conditions on the body surfaces and initial conditions. Several discretization techniques allow for approximating solutions of the set of coupled equations (1-4). For the sake of simplicity, all the following equations refer to a linear thermoelastic system. The resulting semi-discretized set of ordinary differential equations reads,

$$\begin{bmatrix} \mathbf{M}_{uu} & \mathbf{0} \\ \mathbf{0} & \mathbf{0} \end{bmatrix} \begin{bmatrix} \ddot{\mathbf{u}} \\ \ddot{\boldsymbol{\theta}} \end{bmatrix} + \begin{bmatrix} \mathbf{C}_{uu} & \mathbf{0} \\ \mathbf{C}_{\theta u} & \mathbf{C}_{\theta\theta} \end{bmatrix} \begin{bmatrix} \dot{\mathbf{u}} \\ \dot{\boldsymbol{\theta}} \end{bmatrix} + \begin{bmatrix} \mathbf{K}_{uu} & \mathbf{K}_{u\theta} \\ \mathbf{K}_{\theta u} & \mathbf{K}_{\theta\theta} \end{bmatrix} \begin{bmatrix} \mathbf{u} \\ \boldsymbol{\theta} \end{bmatrix} = \begin{bmatrix} \mathbf{F}_u \\ \mathbf{F}_\theta \end{bmatrix} \tag{5}$$

In detail, matrix partitioning refers to displacement and temperature DoFs, i.e. $\mathbf{u}$ and $\boldsymbol{\theta}$, respectively. Accordingly, $\mathbf{M}_{uu}, \mathbf{K}_{uu}$ and $\mathbf{C}_{uu}$ are mass, stiffness and damping matrices; $\mathbf{K}_{\theta\theta}$ and $\mathbf{C}_{\theta\theta}$ are heat conductive and capacity matrices. $\mathbf{F}_u$ and $\mathbf{F}_\theta$ vectors represent mechanical and thermal loads, respectively, where positive thermal fluxes $\mathbf{F}_\theta$ supply energy to the system, whilst negative subtract energy from the system.
Since the out-of-diagonal block submatrix $\mathbf{K}_{u\theta}$ provides internal forces owing to restrained thermal deformations, it is crucial to account for thermomechanical structural interactions. $\mathbf{K}_{\theta u}$ accounts for thermal load changes due to mechanical behavior. This is the case when cover spalling in concrete structural elements occurs and reinforcement bars are directly exposed to the thermal action of fire or when the specimen undergoes large deformations in a compartment with non-uniform temperature, e.g. the floor deflects down towards the fire or a beam twists changing the exposure from the flange to the web. Finally, $\mathbf{C}_{\theta u}$ represents the heat generation due to strain rate, which is important for micro-scale applications, but negligible for large-scale problems. In this preliminary phase both contributions dictated by terms $\mathbf{C}_{\theta u}$ and $\mathbf{K}_{\theta u}$ were neglected, which means that the mechanical behaviour does not affect the temperature distribution in the solid body. At this stage, the following classification can be helpful:

- **Physics full coupling**: the thermal behavior affects the mechanical behavior and vice versa.
- **Physics partial coupling**: the thermal/mechanical behavior affects mechanical/thermal behavior but not vice versa.

Now, by applying the Hybrid Simulation (HS) technique, each matrix can be partitioned in pure Numerical-, pure Physical- and Boundary-DoFs, respectively, [8]. For brevity, the following simplified notation holds: N-DoFs, P-DoFs and B-DoFs, respectively. The complete derivation of the governing discretized equations entails that,

$$\mathbf{u} = \begin{bmatrix} \mathbf{u}^{N^T} & \mathbf{u}^{B^T} & \mathbf{u}^{P^T} \end{bmatrix}^T, \quad \boldsymbol{\theta} = \begin{bmatrix} \boldsymbol{\theta}^{N^T} & \boldsymbol{\theta}^{B^T} & \boldsymbol{\theta}^{P^T} \end{bmatrix}^T \tag{6}$$

Accordingly, a generic load vector $\mathbf{F}$ reads:

$$\mathbf{F}_u = \begin{bmatrix} \mathbf{F}_u^{N^T} & \mathbf{F}_u^{B^T} & \mathbf{F}_u^{P^T} \end{bmatrix}^T, \quad \mathbf{F}_\theta = \begin{bmatrix} \mathbf{F}_\theta^{N^T} & \mathbf{F}_\theta^{B^T} & \mathbf{F}_\theta^{P^T} \end{bmatrix}^T \tag{7}$$

All matrices must be expanded to all DoFs considered in the emulated system. In the HS practice B-DoFs coincide with P-DoFs [9]. The expanded stiffness and conductivity matrices yield,

$$\mathbf{K}_{uu}^N = \begin{bmatrix} \mathbf{K}_{uu}^N & \mathbf{K}_{uu}^N & \mathbf{0} \\ \mathbf{K}_{uu}^N & \mathbf{K}_{uu}^N & \mathbf{0} \\ \mathbf{0} & \mathbf{0} & \mathbf{0} \end{bmatrix}, \mathbf{K}_{uu}^P = \begin{bmatrix} \mathbf{0} & \mathbf{0} & \mathbf{0} \\ \mathbf{0} & \mathbf{K}_{uu}^P & \mathbf{K}_{uu}^P \\ \mathbf{0} & \mathbf{K}_{uu}^P & \mathbf{K}_{uu}^P \end{bmatrix}, \quad \mathbf{K}_{\theta\theta}^N = \begin{bmatrix} \mathbf{K}_{\theta\theta}^N & \mathbf{K}_{\theta\theta}^N & \mathbf{0} \\ \mathbf{K}_{\theta\theta}^N & \mathbf{K}_{\theta\theta}^N & \mathbf{0} \\ \mathbf{0} & \mathbf{0} & \mathbf{0} \end{bmatrix}, \mathbf{K}_{\theta\theta}^P = \begin{bmatrix} \mathbf{0} & \mathbf{0} & \mathbf{0} \\ \mathbf{0} & \mathbf{K}_{\theta\theta}^P & \mathbf{K}_{\theta\theta}^P \\ \mathbf{0} & \mathbf{K}_{\theta\theta}^P & \mathbf{K}_{\theta\theta}^P \end{bmatrix}, \tag{8}$$

The same criterion applies to remainder of (5). Accordingly, (5) can be split into NS and PS contributions.

$$\begin{bmatrix} \left(\mathbf{M}_{uu}^{N}+\mathbf{M}_{uu}^{P}\right) & \mathbf{0} \\ \mathbf{0} & \mathbf{0} \end{bmatrix}\begin{bmatrix} \ddot{\mathbf{u}} \\ \ddot{\boldsymbol{\theta}} \end{bmatrix}+\begin{bmatrix} \left(\mathbf{C}_{uu}^{N}+\mathbf{C}_{uu}^{P}\right) & \mathbf{0} \\ \mathbf{0} & \left(\mathbf{C}_{\theta\theta}^{N}+\mathbf{C}_{\theta\theta}^{P}\right) \end{bmatrix}\begin{bmatrix} \dot{\mathbf{u}} \\ \dot{\boldsymbol{\theta}} \end{bmatrix}+\ldots$$
$$\ldots\begin{bmatrix} \left(\mathbf{K}_{uu}^{N}+\mathbf{K}_{uu}^{P}\right) & \left(\mathbf{K}_{u\theta}^{N}+\mathbf{K}_{u\theta}^{P}\right) \\ \mathbf{0} & \left(\mathbf{K}_{\theta\theta}^{N}+\mathbf{K}_{\theta\theta}^{P}\right) \end{bmatrix}\begin{bmatrix} \mathbf{u} \\ \boldsymbol{\theta} \end{bmatrix}=\begin{bmatrix} \left(\mathbf{F}_{u}^{N}+\mathbf{F}_{u}^{P}\right) \\ \left(\mathbf{F}_{\theta}^{N}+\mathbf{F}_{\theta}^{P}\right) \end{bmatrix} \tag{9}$$

After simple manipulations of (9), the thermomechanical response of the PS enters the right hand side (RHS) of the balance equation as interface load **R**, i.e. force and heat flux, applied to the NS. With regard to the real-time (RT) case, where a rate dependent response of the PS is expected, (9) becomes,

$$\begin{bmatrix} \mathbf{M}_{uu}^{N} & \mathbf{0} \\ \mathbf{0} & \mathbf{0} \end{bmatrix}\begin{bmatrix} \ddot{\mathbf{u}} \\ \ddot{\boldsymbol{\theta}} \end{bmatrix}+\begin{bmatrix} \mathbf{C}_{uu}^{N} & \mathbf{0} \\ \mathbf{0} & \mathbf{C}_{\theta\theta}^{N} \end{bmatrix}\begin{bmatrix} \dot{\mathbf{u}} \\ \dot{\boldsymbol{\theta}} \end{bmatrix}+\begin{bmatrix} \mathbf{K}_{uu}^{N} & \mathbf{K}_{u\theta}^{N} \\ \mathbf{0} & \mathbf{K}_{\theta\theta}^{N} \end{bmatrix}\begin{bmatrix} \mathbf{u} \\ \boldsymbol{\theta} \end{bmatrix}=\begin{bmatrix} \mathbf{F}_{u}^{N}-\mathbf{R}_{u}^{P} \\ \mathbf{F}_{\theta}^{N}-\mathbf{R}_{\theta}^{P} \end{bmatrix} \tag{10}$$

where,

$$\begin{bmatrix} \mathbf{R}_{u}^{P} \\ \mathbf{R}_{\theta}^{P} \end{bmatrix}=\begin{bmatrix} \mathbf{M}_{uu}^{P} & \mathbf{0} \\ \mathbf{0} & \mathbf{0} \end{bmatrix}\begin{bmatrix} \ddot{\mathbf{u}} \\ \ddot{\boldsymbol{\theta}} \end{bmatrix}+\begin{bmatrix} \mathbf{C}_{uu}^{P} & \mathbf{0} \\ \mathbf{0} & \mathbf{C}_{\theta\theta}^{P} \end{bmatrix}\begin{bmatrix} \dot{\mathbf{u}} \\ \dot{\boldsymbol{\theta}} \end{bmatrix}+\begin{bmatrix} \mathbf{K}_{uu}^{P} & \mathbf{K}_{u\theta}^{P} \\ \mathbf{0} & \mathbf{K}_{\theta\theta}^{P} \end{bmatrix}\begin{bmatrix} \mathbf{u} \\ \boldsymbol{\theta} \end{bmatrix}-\begin{bmatrix} \mathbf{F}_{u}^{P} \\ \mathbf{F}_{\theta}^{P} \end{bmatrix} \tag{11}$$

However, the performance of the transfer system, i.e. furnaces and actuators, can limit the loading rate. Therefore, extended time scales are adopted in the laboratory where the test is slowed down with respect to RT testing. As a result, rate dependent components of the PS response must be accounted for numerically. This is the pseudodynamic (PsD) case and (9) turns into,

$$\begin{bmatrix} \left(\mathbf{M}_{uu}^{N}+\mathbf{M}_{uu}^{P}\right) & \mathbf{0} \\ \mathbf{0} & \mathbf{0} \end{bmatrix}\begin{bmatrix} \ddot{\mathbf{u}} \\ \ddot{\boldsymbol{\theta}} \end{bmatrix}+\begin{bmatrix} \left(\mathbf{C}_{uu}^{N}+\mathbf{C}_{uu}^{P}\right) & \mathbf{0} \\ \mathbf{0} & \left(\mathbf{C}_{\theta\theta}^{N}+\mathbf{C}_{\theta\theta}^{P}\right) \end{bmatrix}\begin{bmatrix} \dot{\mathbf{u}} \\ \dot{\boldsymbol{\theta}} \end{bmatrix}+\begin{bmatrix} \mathbf{K}_{uu}^{N} & \mathbf{K}_{u\theta}^{N} \\ \mathbf{0} & \mathbf{K}_{\theta\theta}^{N} \end{bmatrix}\begin{bmatrix} \mathbf{u} \\ \boldsymbol{\theta} \end{bmatrix}=\begin{bmatrix} \mathbf{F}_{u}^{N}-\mathbf{R}_{u}^{P} \\ \mathbf{F}_{\theta}^{N}-\mathbf{R}_{\theta}^{P} \end{bmatrix} \tag{12}$$

where,

$$\begin{bmatrix} \mathbf{R}_{u}^{P} \\ \mathbf{R}_{\theta}^{P} \end{bmatrix}=\begin{bmatrix} \mathbf{K}_{uu}^{P} & \mathbf{K}_{u\theta}^{P} \\ \mathbf{0} & \mathbf{K}_{\theta\theta}^{P} \end{bmatrix}\begin{bmatrix} \mathbf{u} \\ \boldsymbol{\theta} \end{bmatrix}-\begin{bmatrix} \mathbf{F}_{u}^{P} \\ \mathbf{F}_{\theta}^{P} \end{bmatrix} \tag{13}$$

The first block row of (10) and (12), without the coupling term $\mathbf{K}_{u\theta}$, has been deeply investigated for many years and extensively used in the seismic domain. Conversely, the second row-block still deserves particular attention. In fact, it determines the thermal coupling between NS and PS. In principle, compatibility of primal quantities -displacements, temperatures- and balance of dual quantities -forces, heat fluxes- must hold across the interface between the NS and the PS. This means that an accurate temperature control is needed for applying a prescribed temperature field at the interface of the PS and the corresponding heat fluxes should feedback to the NS. Nevertheless, some constraint can be potentially relaxed allowing for easier implementations. For the sake of clarity, a couple of definitions is given about strength of coupling between PSs and NSs:

- **Substructures full coupling**: displacements/temperatures are sent from the NS to PS and interface forces/heat fluxes are sent back from the PS to the NS.

- **Substructures partial coupling**: the same as full coupling forces/heat fluxes are not sent back to the NS from the PS.

In this respect, the paper focuses on the second row block of (9) from the hybrid simulation perspective, i.e. substructure thermal coupling. Therefore, a rigorous coupling among "physical" – here numerically emulated - and numerical subdomains is investigated through numerical simulations.

3 THE ILLINOIS BRIDGE REFERENCE CASE STUDY

From the perspective of the development of a full THS, a proof-of-concept case study was selected. The 5.6 m long, truss bridge mock-up model, which was tested at the Smart Structures Technology Laboratory (SSTL) of the University of Illinois at Urbana-Champaign [10], was taken as reference structural system, as illustrated in Figures 1 and 2. A typical fire scenario for such a structure can be a burning truck on the carriageway. The length of each bay of the truss is 0.4 m on each side. The thermal physics was considered only.

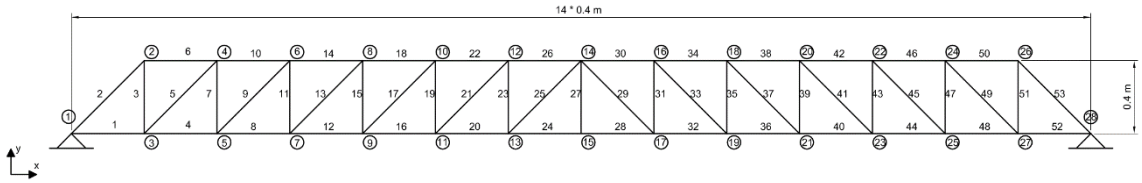

Fig. 1 - Scheme of the Matlab 2D FE model based on thermal truss elements with numbering enabled.

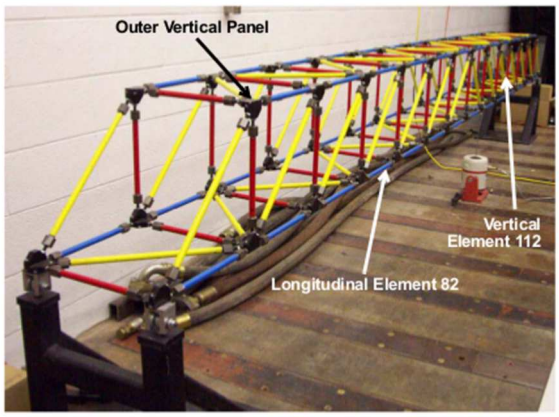

Fig. 2 - Mock-up model of the reference truss bridge case study.

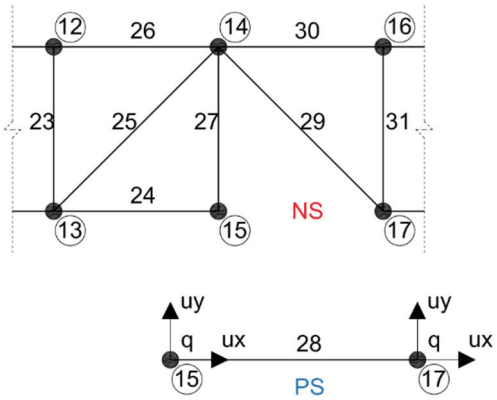

Fig. 3 - Substructuring scheme: Element #28 is substructured in the laboratory.

As can be appreciated from Figure 3, a single 2D truss element is substructured in the laboratory. A Könn STE-12 HR/350' electrical furnace (Könn Furnace in Figure 4a), which encapsulated the 1:5 scale specimen of the substructured truss of Figure 4b, controls temperatures using three West 8100+ Single Loop Controllers (West 8100). This provides the ability to control temperature in three zones. Although uniform temperature fields characterize the specimen in this preliminary study, thermal gradients can be potentially applied to the substructured element. The furnace is capable of heating at a rate of 60 degrees/minute up to 600 degrees and 40 degrees/minute up to 1100 degrees. A Zwick 1484 Universal Testing Machine (Zwick UTM) holds the specimen.

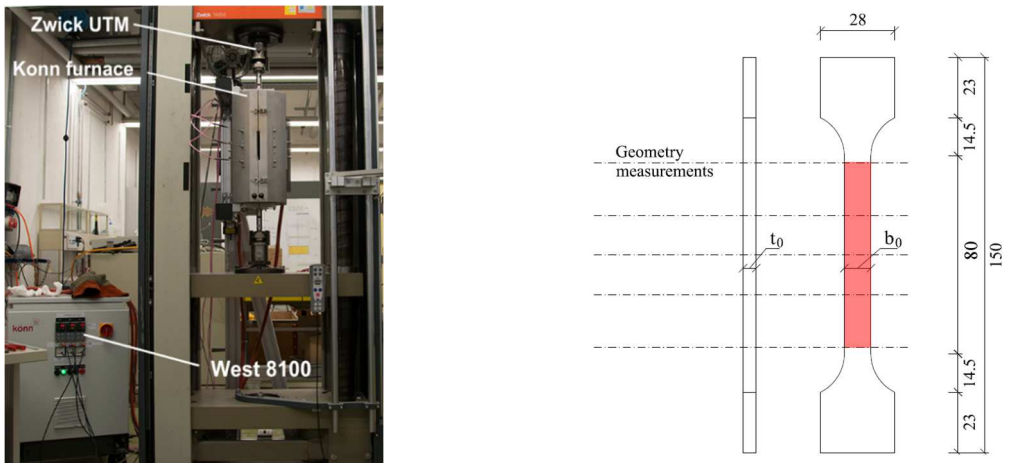

a b

Fig. 4 - a) Zwick UTM and Könn Furnace test setup; b) schematic of the dog-bone specimen including the geometric values in mm.

Temperature feedbacks are measured from both ends of the specimen. The Zwick UTM and Könn furnace had existing controllers with a Zwick/Roell testXpert II Software user interface [11]. An INDEL RT computer runs a Simulink model that handles both the controller as well as the THS software. Figure 4b shows the geometry of the test specimen. Since grips hold specimen's ends, the highlighted portion, is considered as the scaled substructured truss for the purpose of THS. The nominal width b_0 of the specimen measures 10 mm, whilst the nominal thickness t_0 measures 5 mm. The total length is 80 mm. Therefore, the specimen is consistent with the substructured truss with a geometric scaling factor δ equal to 5. A pair of thermocouples at each end of the specimen allows for estimating temperature gradients, and therefore feedback heat fluxes.

3.1 FE model of the reference case study

A linear 2D FE model of the bridge consisting of 53 thermal truss elements and 28 nodes was implemented in Matlab. According to Figure 1, structural nodes are numbered starting from left to right, with all the odd numbers at the lower chord, and all the even numbers at the upper chord, except node 28 which is at the right support. Each structural node number has a circle around it. All elements are characterized by a circular cross section with an inner diameter of 1.09 cm and an outer diameter of 1.71 cm except Elements #24 and #28, which have 2.50 x 5.00 cm rectangular solid cross sections. Uniform steel material properties were considered for the all bridge truss elements. Table 1 summarize steel material parameters characterizing the bridge that for simplicity were kept constant with temperature:

Table 1. Steel material parameters characterizing bridge trusses.

Description	Symbol	Value	Unit
Density	ρ	7800	[kg/m3]
Thermal conductivity	k	43	[W/m/K]
Thermal capacity	c_p	445	[J/kg/K]

In order to keep the problem linear, thermal radiation was neglected. Conversely, heat transfer by convection was considered at each node. An equivalent exchanging surface S of 0.80 m^2 was considered for all related elements. In order to investigate the influence of each heat transfer mechanism on the analyzed problem, two case studies were defined: Case Study #1 considers a convective coefficient h equal to 50 $W/(m^2K)$ and steel material properties; Case Study #2 analyses the problem with reduced density of 78 kg/m^3 and convective coefficient h equal to 1 $W/(m^2K)$. A significant reduction of density entails a much higher thermal diffusivity (from 11 mm^2/s typical of steel to 1200 mm^2/s typical of pyrolytic graphite) and a smaller Biot number for Case Study #2 than Case Study #1. This means that relative to Case Study #1, in Case Study #2 the resistance to heat transfer offered by conduction is less with respect to convection. The ANSYS FE code was taken as reference for the validation of the developed Matlab FE library.

3.2 Refined numerical modelling of the THS environment

HS was extensively applied for determining the seismic response of a prototype structure. In detail, the substructure, whose behavior is known, is modeled numerically - NS -, while the portion of the structure whose behavior is highly nonlinear or not well-understood is tested in the laboratory - PS -. The resulting hybrid model consists of numerical and physical subdomains that interact at each time step of the solution of the equation of motion for an applied dynamic excitation. The control software and the specimen actuation system enforce consistent boundary conditions at the interface between the substructures. The same philosophy applies to the thermal case. Here in the current preliminary phase, an axisymmetric COMSOL FE model simulates the thermal response of the "experimental" substructure inside the Könn Furnace. This approach allows for reliable estimates of actual heat fluxes coming from the truss specimen, which account for furnace leakage; thus, providing realistic insight into the capabilities of THS. The axisymmetric approach allows for reducing the total number of DoFs. Figure 5a reports the reference slice of the axisymmetric COMSOL FE model, whilst Figure 5b, shows the FE model in the revolved 3D domain.

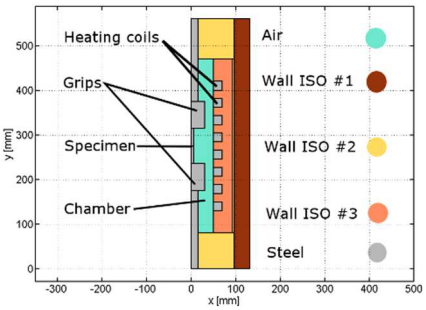

Fig. 5a - Scheme of the reference slice of the axisymmetric COMSOL FE model.

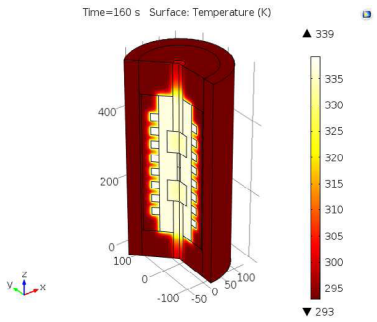

Fig. 5b - Temperature response of the COMSOL FE model in the revolved domain.

The PS in the 3D revolved domain, here numerically simulated, is characterized by the same lateral surface of the physical truss, which has a rectangular solid cross section. Therefore, an equivalent radius equal to 4.77 mm was considered. All furnace characteristics, included dimensions and material properties, were obtained from the manufacturer and are summarized in Table 2.

Table 2. Material parameters characterizing the COMSOL FE model of the furnace.

Material	Density $[kg/m^3]$	Specific heat $[J/(kgK)]$	Thermal conductivity $[W/(mK)]$
Wall ISO#1	300	1050	0.020
Wall ISO#2	128	1130	0.060
Wall ISO#3	880	1100	0.300
Steel (specimen and grips)	7800	466	43
Air (chamber)	1.25	1005	0.024

The thermal load was applied to the heating coil domain in terms of heat source per unit volume. A maximum total power of 6 kW was allowed according to the furnace datasheet. Since air is a very good thermal isolator, the most of heat transfer is caused by mass transportation of convective flows, which mix air from cold and hot regions of the chamber subdomain. Therefore, mixing is crucial to replicate a realistic furnace behavior. To this end, an isothermal constraint was applied to the air subdomain. In order to preserve linearity, the radiation contribution was neglected. Nevertheless, all approximations have proven to be satisfactory and the COMSOL FE model replicates the Könn Furnace response without a need for a Computational Fluid Dynamics (CFD) simulation in the temperature range of interest, i.e. 300-600 K. Figure 6 depicts a contour plot of the temperature response of the Könn Furnace subjected to maximum input power after 100 s. Black arrows represent heat flux streamlines. Figure 7 offers a close up view on the specimen domain, where interface temperatures and exchanged heat fluxes are indicated.

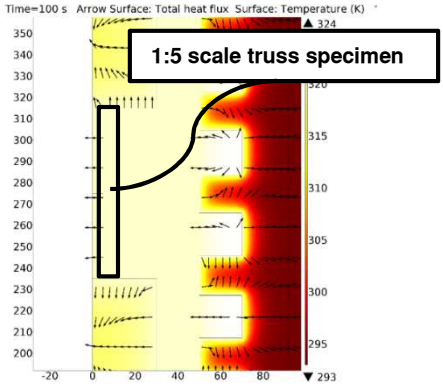

Fig. 6 - Contour plot of the temperature response of the furnace. Black arrows represent thermal flux streamlines.

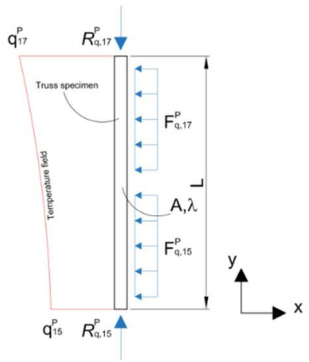

Fig. 7 - Schematic of thermal fluxes applied to the 1:5 scale truss specimen. Vector orientations must be intended as positive according to (8-11).

According to Figure 6, the heat fluxes $\mathbf{F}_{q,15}^{P}$ and $\mathbf{F}_{q,17}^{P}$ enter the specimen through the chamber and flows out to grips at both the specimen ends. Thus, negative heat fluxes $\mathbf{R}_{q,15}^{P}$ and $\mathbf{R}_{q,17}^{P}$ are expected at both ends of the specimen, which interface the PS to the NS.

In order to simulate the overall HS environment, the same PI control strategy of the Könn furnace was implemented and the developed COMSOL FE model simulated the plant. Since fire engineers are used to defining thermal loads in terms of time-temperature fire curves, a hybrid compatible Differential Algebraic Equation (DAE) solver was implemented. It is based on a dual formulation where a set of Lagrange multipliers can impose prescribed trajectories on derivatives of state quantities. Such an approach preserves the stability of the underlying time

stepping scheme. In this particular case the trapezoidal rule was selected as reference algorithm, and the following DAE was taken as a model problem,

$$\begin{aligned} &\mathbf{C}_{\theta\theta}\dot{\boldsymbol{\theta}}+\mathbf{K}_{\theta\theta}\boldsymbol{\theta}=\mathbf{F}_{\theta}(t)+\mathbf{L}_{\theta}^{T}\boldsymbol{\lambda}_{\theta}(t) \\ &\mathbf{L}_{\theta}\dot{\boldsymbol{\theta}}=\mathbf{c}_{\theta}(t) \end{aligned} \tag{14}$$

where the Lagrange multiplier vector $\boldsymbol{\lambda}_q$ consists of additional fictitious heat fluxes that force the temperature response to follow prescribed rates dictated by $\mathbf{c}_{\boldsymbol{q}}(t)$. $\mathbf{L}_q$ is a Boolean matrix that localizes constrained DoFs and, therefore, localizes Lagrange multipliers on the load vector.

4 NUMERICAL SIMULATION OF THS

Several numerical simulations of the proposed THS architecture were executed considering different extended time scales λ. The devised PI controller was selected to impose temperature at furnace nodes by modulating the input heat power of heating coils in the COMSOL FE model of the Könn Furnace. A thermal load case was defined based on the international standard ISO 834 temperature-time fire curve, which is defined in the Eurocode 1 Part 1-2 [12] as:

$$\theta_g = 20+345\cdot\log_{10}(8\cdot t+1) \tag{15}$$

where θ_g is gas or air temperature (°C) and t is time (min). For simplicity, the aforementioned ISO 834 time-temperature curve was applied to the Nodes #13, #15 and #17 of the hybrid model of the truss bridge as temperature history even though in reality the temperature of the element will not exactly follow the heating curve. SI units will be used in the following. Indeed temperature are expressed in K.

a b

Fig. 8 - ISO 834 time - temperature curve: a) time vs. temperature; b) time vs. temperature rate

Since entailing temperature rate exceeds the Könn Furnace capabilities, which negates for values greater than 1 K/s, an extended time scale λ was considered in the simulated laboratory. Therefore, the test was slowed down of a factor λ and the PS experienced a simulation time step Δt in $\lambda\Delta t$ of wall clock time. In order to investigate the effects of time scaling, a 2-DoFs thermal truss model of the sole 1:5 scale steel specimen was implemented. Material parameters refer to steel; see Table 1 in this respect, whilst geometric values refer to the 1:5 scale truss specimen of Figure 4b. A convective coefficient h equal to 10 $W/(m^2K)$ was considered as a reasonable value. Time constants derived from the 2-DoFs model of the 1:5 scale specimen are 110.56 s and 605.80 s. Since temperature histories were imposed at both specimen ends,

estimations of both rate dependent and rate independent components of thermal fluxes, i.e. $\mathbf{R}_q^{P,RD}$ and $\mathbf{R}_q^{P,RI}$, were estimated,

$$\begin{aligned}\mathbf{R}_\theta^{P,RD} &= \frac{\mathbf{C}_{\theta\theta}^P \dot{\boldsymbol{\theta}}}{\lambda} \\ \mathbf{R}_\theta^{P,RI} &= \mathbf{K}_{\theta\theta}^P \boldsymbol{\theta}\end{aligned} \tag{16}$$

where $\mathbf{C}_{\theta\theta}^P$ and $\mathbf{K}_{\theta\theta}^P$, are the heat capacity and the conductivity matrices of the 2-DoFs model of the specimen, respectively. Superscripts RD and RI stand for rate dependent and rate independent, respectively. Since the experimental time scale λ affects temperature rates, it reflects on the corresponding heat flux $\mathbf{R}_q^{P,RD}$. Figure 9 reports time histories of both the components. In particular, Figure 9c focuses on rate dependent components for time scaling λ greater than one.

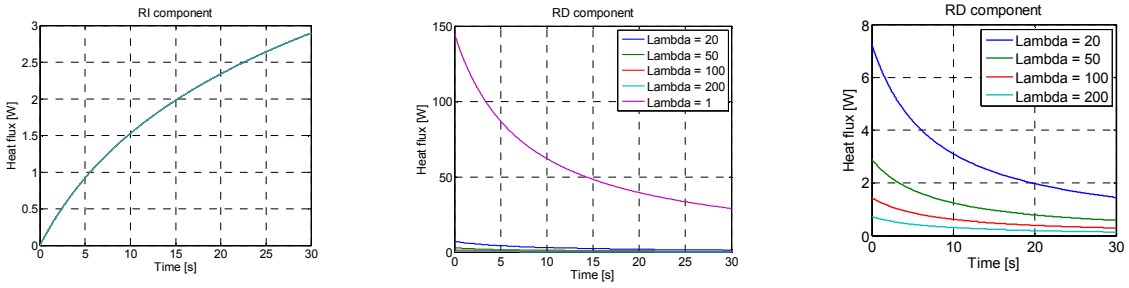

a b c

Fig. 9 - Time histories of feedback heat fluxes components: a) rate independent contribution $\mathbf{R}_q^{P,RI}$; b) rate dependent contribution $\mathbf{R}_q^{P,RD}$; close up view on rate dependent contribution $\mathbf{R}_q^{P,RD}$ in the case of extended time scales

From Figure 16 it is possible to observe that time scalings, which are compatible with the performance of the Könn Furnace, cancel rate dependent contributions, which must be taken into account numerically in the NS. This is the analogous to pseudodynamic (PsD) testing where rate dependent forces, e.g. inertia and viscous damping, are simulated numerically. Estimates of feedback heat fluxes retrieved from the COMSOL FE model were magnified according to the geometric scale factor δ, and accounted for in the thermal balance equation (10-11). A simple proof of this approach can be derived from the Fourier law in the one-dimensional case,

$$\Phi' = -\lambda A \delta^2 \frac{dT}{\delta dx} = \Phi \delta \tag{17}$$

where Φ' and Φ are heat fluxes related to the full scale model and the scaled specimen, respectively. As can be appreciated from Figure 10, which reports feedback heat fluxes retrieved from the COMSOL, transient dynamics occurs at the beginning of the simulation for all values of time scale λ. Their lengths are constant in the laboratory time and of the same order of magnitude of the lower thermal time constant of the sole specimen, which was estimated at 110 s. Therefore, they can be ascribed to a local transient thermal response of the

furnace/specimen. Figure 11 report the temperature responses of Node #17, which corresponds to the upper node of the specimen, for the Case Study #1.

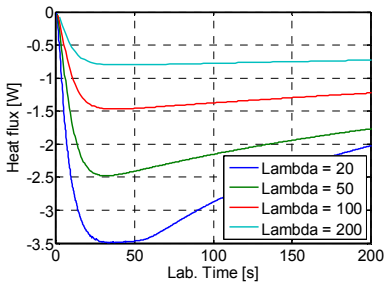

Fig. 10 - Feedback heat flux measured at the upper end of the 1:5 scale specimen on the COMSOL FE model vs. laboratory time (wall clock) for the Case Study #1

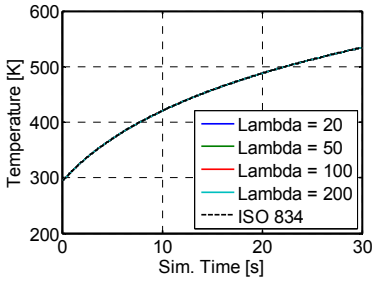

Fig. 11 - Temperature response of Node #15 for different values of time scale λ for the Case Study #1.

As can be appreciated from Figure 11, the devised THS allowed for applying the correct temperature path and simulating the global system response in a consistent manner. Potential aftermath of substructures partial and full coupling can be deducted more clearly by Lagrange multipliers behavior. In greater detail, Figure 12 reports the time histories of the Lagrange multiplier applied at Node #15, where the ISO 834 was prescribed for both the case studies.

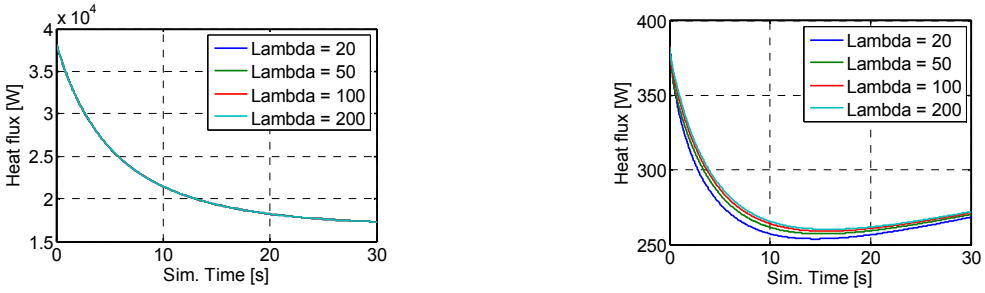

a b

Fig. 12 - Time histories of Lagrange multipliers at Node #15 for different values of time scale λ for: a) Case Study #1; and b) Case Study #2.

In detail, Figure 12a, which refers to Case Study #1, describes that when thermal diffusivity is on the order of 12 mm^2/s and h/k = 1.16 m/m, specimen feedback heat fluxes are negligible because no effects can be appreciated on Lagrange multipliers that impose the temperature path on Node #15 as fictitious heat fluxes. As a consequence, a substructure partial coupling can be applied. Conversely, from Figure 12b, which refers to Case Study #2, when thermal diffusivity is on the order of 1200 mm^2/s and h/k = 0.02 m/m, feedback heat fluxes affect the dynamic solution and should be taken into account.

5 CONCLUSIONS AND FUTURE PERSPECTIVES

The present paper summarizes all research activities focused on the development of a pure THS. The full set of coupled equations defining the thermomechanical problem was discussed from the HS perspective and particular care was given to the heat transfer physics. The study highlights the feasibility of the THS by applying an arbitrary temperature path to both case

studies and simulating the global system response in a consistent manner. Results have shown that specimen feedback heat fluxes can be neglected in the global heat balance when an is element characterized by thermal diffusivity on the order of 12 mm^2/s - Case Study #1 – and $h/k \approx 1$. Therefore, a substructure partial coupling can be applied. Conversely, when thermal diffusivity is higher (1200 mm^2/s) and conduction offers very little resistance to heat transfer with respect to convection ($h/k << 1$) - Case Study #2 -, feedback fluxes affect the dynamic solution and must be taken into account using a substructure full coupling. A forthcoming experimental campaign will allow for updating the developed simulation environment and tuning an effective testing protocol. The presented approach provides a realistic insight into the capabilities of THS and paves the way for simulating hot NSs for the purpose of TMHS.

REFERENCES

[1] Mostafaei, H. (2013a). Hybrid fire testing for assessing performance of structures in fire -Application. Fire Safety Journal, 56, 30–38. doi:10.1016/j.firesaf.2012.12.003

[2] Mostafaei, H. (2013b). Hybrid fire testing for assessing performance of structures in fire -Methodology. Fire Safety Journal, 58, 170–179. doi:10.1016/j.firesaf.2013.02.005

[3] Franssen, J. M. (2005). SAFIR: A thermal/structural program for modeling structures under fire. Engineering Journal-American Institute of Steel Construction Inc, 42(3).

[4] Whyte, C. A., K.R. Mackie, and B. Stojadinovic, (2014). Hybrid Simulation of Thermomechanical Structural Response. ASCE Journal of Structural Engineering (in review).

[5] OpenFresco, (2014). Open Framework for Experimental Setup and Control. http://openfresco.neesforge.nees.org.

[6] OpenSees, (2014). Open System for Earthquake Engineering Simulation. http://opensees.berkeley.edu.

[7] Eslami, M., & Richard, B. (2008). Thermal Stresses: Advanced Theory and Applications.

[8] Shing, P. B. (2008), "Real-time hybrid testing techniques" in Modern testing techniques for structural systems Bursi O.S., Wagg D.J.E. (eds.), CISM International Centre for Mechanical Sciences, vol 502. Springer, Vienna.

[9] Bursi, O.S., Buelga, A.G., Vulcan, L., Neild, S.A. and Wagg, D.J. (2008), "Novel coupling Rosenbrock-based algorithms for real-time dynamic substructure testing", Earthquake Engineering and Structural Dynamics, 37:339-360.

[10] Yong Gao, Billie F. Spencer, Jr., (2008). Structural Health Monitoring Strategies for Smart Sensor Networks Report Series Report No. NSEL-011 Department of Civil and Environmental Engineering University of Illinois at Urbana-Champaign.

[11] Pauli, J., Somaini, D., Knobloch, M., Fontana, M., (2012). "Experiments on steel columns under fire conditions." Institute of Structural Engineering Technical Report 340, Swiss Federal Institute of Technology, Zurich, Switzerland.

[12] European Committee for Standardization (CEN). (2002). "EN1991-1-2, Eurocode 1: Actions on structures – Part 1-2: General actions – Actions on structures exposed to fire," Brussels.